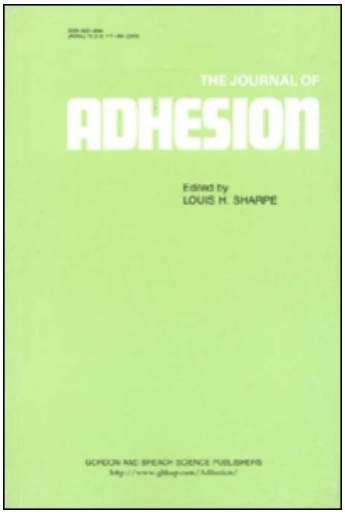

The Journal of Adhesion

Publication details, including instructions for authors and subscription information:
http://www.informaworld.com/smpp/title~content=t713453635

A Fracture Mechanics Approach to Characterizing Cyclic Debonding of Varied Thickness Adhesive Joints to Electroprimed Steel Surfaces

David W. Schmueser[a]
[a] Engineering Mechanics Department, General Motors Research Laboratories, Warren, Michigan, U.S.A.

To cite this Article Schmueser, David W.(1991) 'A Fracture Mechanics Approach to Characterizing Cyclic Debonding of Varied Thickness Adhesive Joints to Electroprimed Steel Surfaces', The Journal of Adhesion, 36: 1, 1 — 23
To link to this Article: DOI: 10.1080/00218469108026520
URL: http://dx.doi.org/10.1080/00218469108026520

J. Adhesion, 1991, Vol. 36, pp. 1–23
Reprints available directly from the publisher
Photocopying permitted by license only

Printed in the United Kingdom

A Fracture Mechanics Approach to Characterizing Cyclic Debonding of Varied Thickness Adhesive Joints to Electroprimed Steel Surfaces*

DAVID W. SCHMUESER

Engineering Mechanics Department, General Motors Research Laboratories, Warren, Michigan 48090-9055, U.S.A.

(Received January 28, 1991; in final form June 3, 1991)

Applications of adhesive bonding for automotive structures have been increasing in recent years due to improvements in the types of adhesives available and in improved knowledge of bonding procedures. Consequently, there exists a demand for design techniques to assess the influence of bondline thickness on adhesive joint strength. One design approach currently being used is based on limiting shear stresses in the adhesive while designing to eliminate peel stresses. Another design approach is based on fracture mechanics and accounts for shear and peel stresses and both static and fatigue modes of failure. The present study applies fracture mechanics to investigate the mixed-mode response of cracked-lap-shear (CLS) joints bonded with unprimed and electroprimed steel surfaces. Three bondline thicknesses equal to 0.254, 0.813, and 1.27 mm were evaluated for unprimed and primed bondlines. For the experimental portion of the study, debond growth rates (da/dN) were measured using a remote imaging system over a range of applied cyclic loads. Corresponding changes in the strain release rates (ΔG) were calculated, through finite element analyses, as a function of debond length and applied load level. The computations for ΔG applied a finite element formulation to determine both the peel component, ΔG_i, and the shear component, ΔG_{ii}. When computed ΔG values were plotted against the measured debond growth rates, da/dN, the results showed a power law relationship which characterizes the debond behavior of a given material system and bondline thickness.

KEY WORDS Cracked-lap-shear joint; cyclic debonding; finite element analysis; strain energy release rate; electropriming; bondline interface.

INTRODUCTION

Automotive applications of adhesives have been increasing in recent years due to improvements in adhesive materials and in improved knowledge of bonding procedures. However, optimum design of adhesively bonded structures will be obtained only when adequate understanding of bondline thickness effects on joint strength and failure modes is achieved. Recent studies conducted at the General Motors

*Presented at the 14th Annual Meeting of The Adhesion Society, Inc., Clearwater, Florida, U.S.A., February 17–20, 1991.

Research Laboratories have applied fracture mechanics concepts to investigate bondline thickness effects on static strengths of unprimed and electroprimed cracked-lap-shear (CLS) joints.[1] The CLS specimen represents mixed-mode (combined peel and shear stress) joint behavior for large area bonds that are typical of many structural applications. The magnitude of each component of this mixed-mode loading can be modified by changing the relative thicknesses of the joint adherends. Investigation of debond behavior for different mode mixes is needed to develop accurate failure criteria for adhesively-bonded joints.

In addition to bondline thickness effects, a better understanding of adhesive joint fatigue behavior is needed. When an adhesively bonded joint is subjected to cyclic loads, one of the several possible damage modes that can occur is the progressive separation of bond between adherends. This is commonly referred to as cyclic debonding. Basic concepts from fracture mechanics have proven successful in modeling cyclic debonding of structural joints.[2–5] All of these studies were directed at joints having bondline thickness values typical of aerospace components (0.08–0.2 mm). However, bondline thicknesses for automotive structural applications typically range from 0.254 mm to 1.5 mm. Therefore, the purpose of the present study was to investigate the manner in which bondline thickness affects the relationship between cyclic joint load and debond growth. Three CLS bondline thicknesses equal to 0.305, 0.813, and 1.27 mm were evaluated. Cyclic load values were input to finite element analyses which compute debond parameters that represent joint resistance to debond growth. Cyclic debonding of the CLS joint is then represented by relating the experimental debond growth rates to the computed debond parameters.

The following sections describe the experimental and computational procedures that were employed to characterize cyclic debonding of unprimed and primed CLS joints.

EXPERIMENTAL CHARACTERIZATION OF BONDLINE MATERIALS AND CYCLIC DEBOND GROWTH

The adhesive used for this study was a one-part epoxy adhesive (Ciba-Geigy Araldite XB-3131), cured according to the manufacturer's instructions. The primer was a proprietary formulation used in GM manufacturing facilities. Tensile properties of the primer material were obtained by testing coupon samples of the thin material removed from a primed surface with a sharp blade. The $102 \times 13 \times 0.2$ mm specimens were tested at room temperature in accordance with ASTM D882, using an Instron Model 1125 machine at a crosshead speed of 3 mm/min. Serrated grips were used in conjunction with pressure-sensitive tape tabs to secure the specimen. Adhesive tensile specimens were cut from cast sheets. The $254 \times 25 \times 3$ mm specimens were tested at room temperature in accordance with ASTM D638, using an MTS Model 810 machine at a crosshead speed of 3 mm/min. Rigid end tabs were employed to reinforce the ends of the mechanically-gripped coupons. Moduli for the primer and adhesive materials, calculated from the initial slope of the stress-strain curves, are listed in Table I.

TABLE I
Adhesive and primer elastic properties

Material	Modulus (GPa)	Poisson's ratio	Adhesive/primer modulus ratio
One-part epoxy	2.83	0.37	2.18
Primer	1.3	0.37	—

Equal thickness (2.54 mm), mild 1010 steel adherends were used for the CLS joints. The lengths of the strap and lap adherends were 305 and 254 mm, respectively (Fig. 1a). The relative thicknesses of the adhesive and primer layers in the bonded specimens are illustrated in Fig. 1b. Unprimed specimens were cut from bonded steel panels that had been degreased with trichloroethane prior to bonding. For the primed specimens, the steel panels were zinc-phosphated before the priming process was completed. Steel wires with diameters equal to 0.254, 0.762, and 1.25 mm were

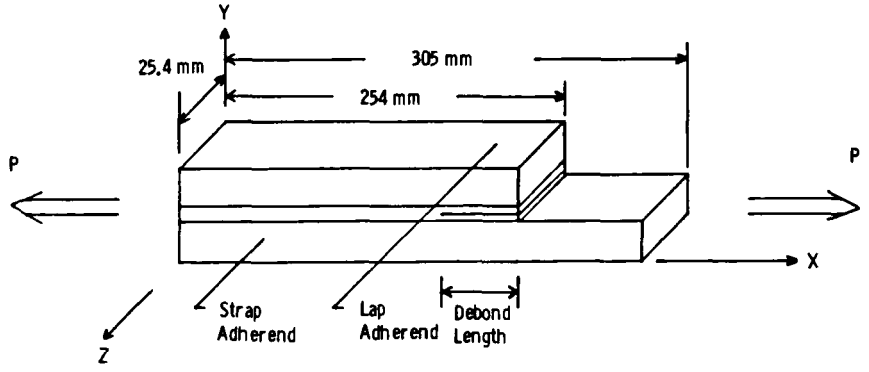

a)

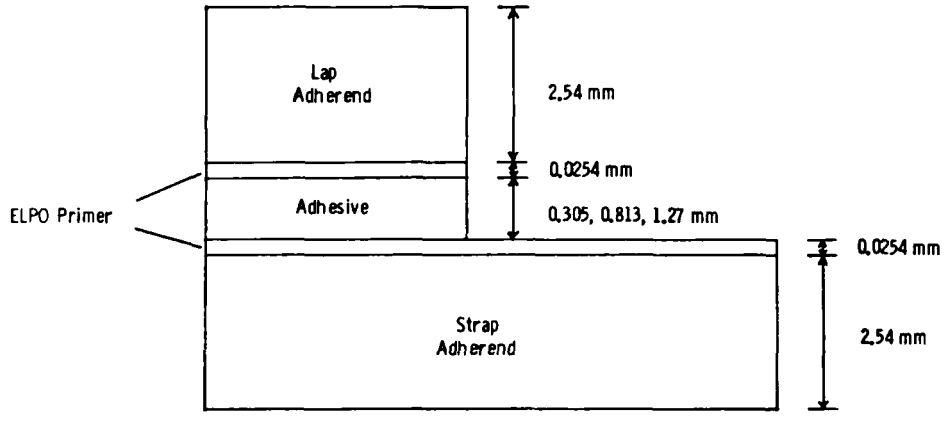

b)

FIGURE 1 CLS Joint Geometry: a), specimen Dimensions; b), Bondline Thickness.

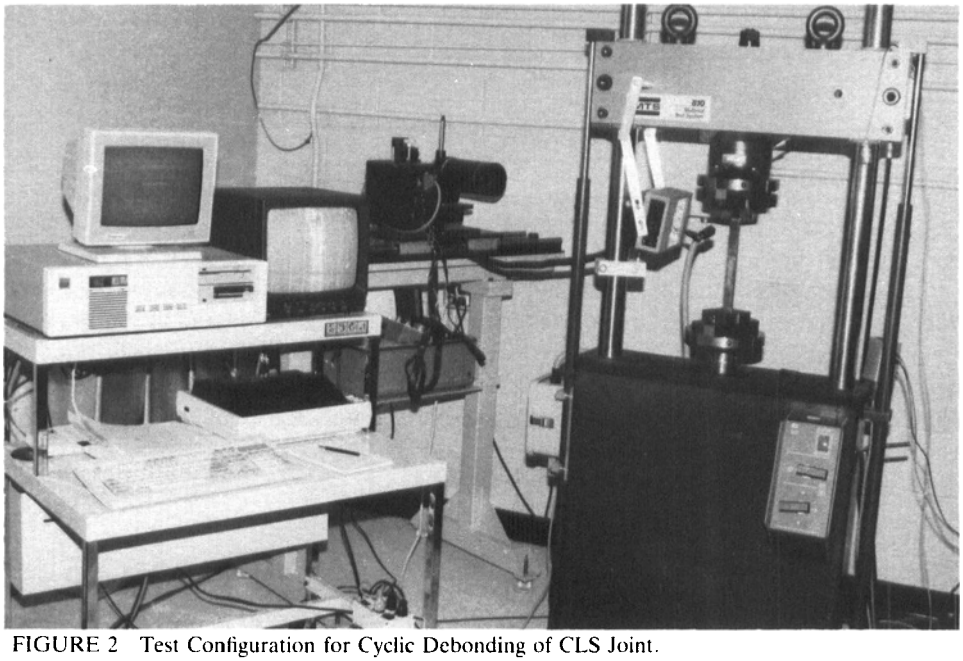

FIGURE 2 Test Configuration for Cyclic Debonding of CLS Joint.

used as spacers to maintain uniform bondline thickness for the cured panels. The specimens were tension-tension tested on an MTS Model 810 machine at room temperature with a stress ratio (P_{min}/P_{max}) of 0.1 and a frequency of 10 Hz. The extent of the cyclic debond length was monitored optically using a remote imaging system (Fig. 2). Typical debond length *versus* fatigue cycle curves are illustrated in Fig. 3 for unprimed and primed CLS specimens.

The possible failure modes in a cyclically-loaded CLS joint are adherend failure (metal yield), cohesive failure within the adhesive, or adhesive failure at a bond interface. All specimens in the present study failed adhesively. The unprimed joints debonded at the adhesive/steel interface, while the primed joints debonded at the primer/steel interface. Debond initiation and growth characteristics for a primed CLS specimen are shown in Fig. 4. A thin groove is machined into the bondline edge, as illustrated in Fig. 4a, to provide a stress concentrator to initiate debond growth. Upon initiation, the debond typically grows immediately toward the strap adherend bondline interface (Fig. 4a). The debond continues to grow in an adhesive manner, as shown in Fig. 4b. This behavior was also observed and analyzed by Mall, Johnson, and Everett.[4] For specimens with the 1.27 mm bondline thickness, debond growth occasionally originated at the interface on the lap side of the specimen, but always reverted to the strap side after growing less than 50 mm (Fig. 5a). Tests were conducted until the debond had grown approximately 100 mm along the specimen. Significant opening of the debond front at the point of crack initiation occurred at maximum debond growth, as illustrated in Fig. 5b.

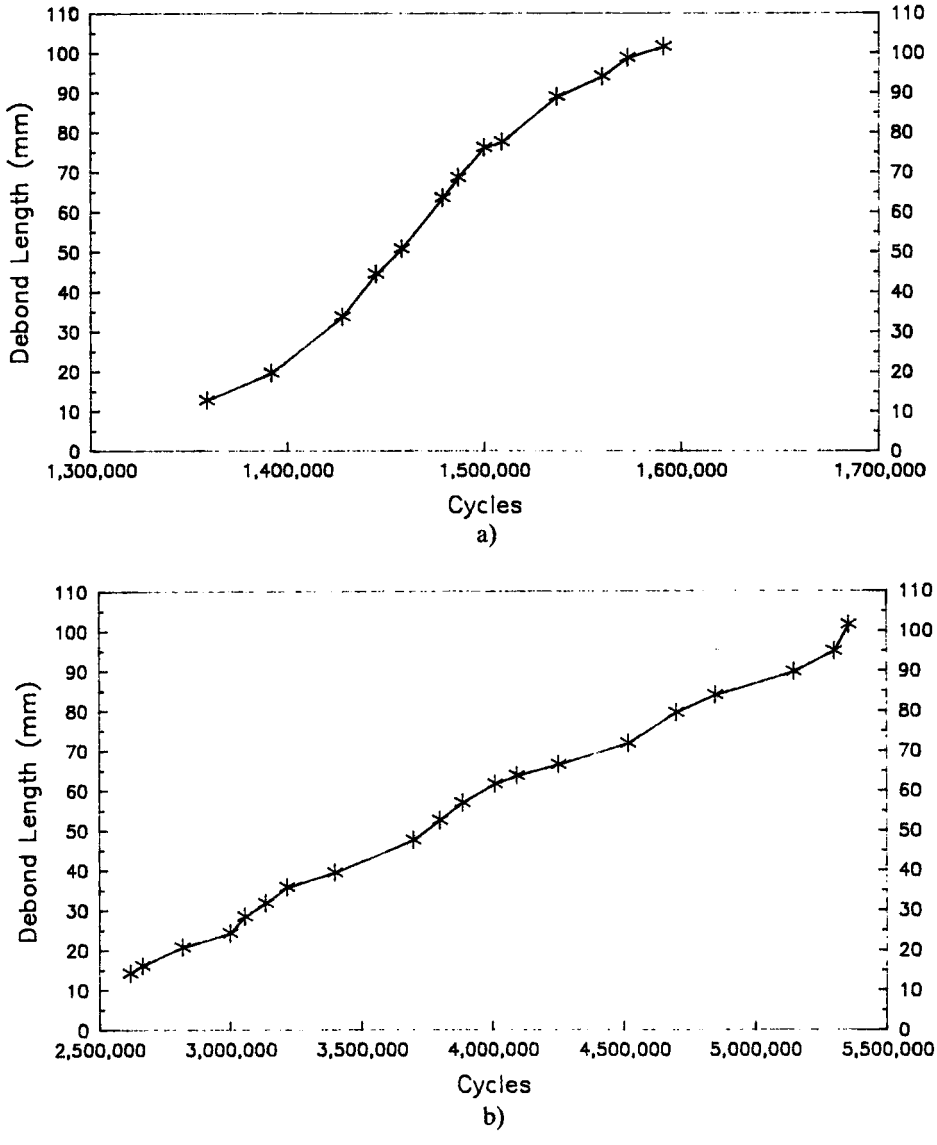

FIGURE 3 Typical Debond Length *vs.* Fatigue Cycles for a) Unprimed and b) Primed Joints (Bondline Thickness = 1.27 mm, P_{max} = 12.0 kN).

FINITE ELEMENT ANALYSIS

The CLS joint geometry was analyzed with a singular finite element (SFE) method[6] to compute debond parameters (strain energy release rates) for given bondline thickness, debond length, and load. The plane strain analyses accounted for geometric nonlinearities that are associated with large rotations. The following presents a brief description of the finite element modeling procedures and the formulation for computing the strain energy release rates.

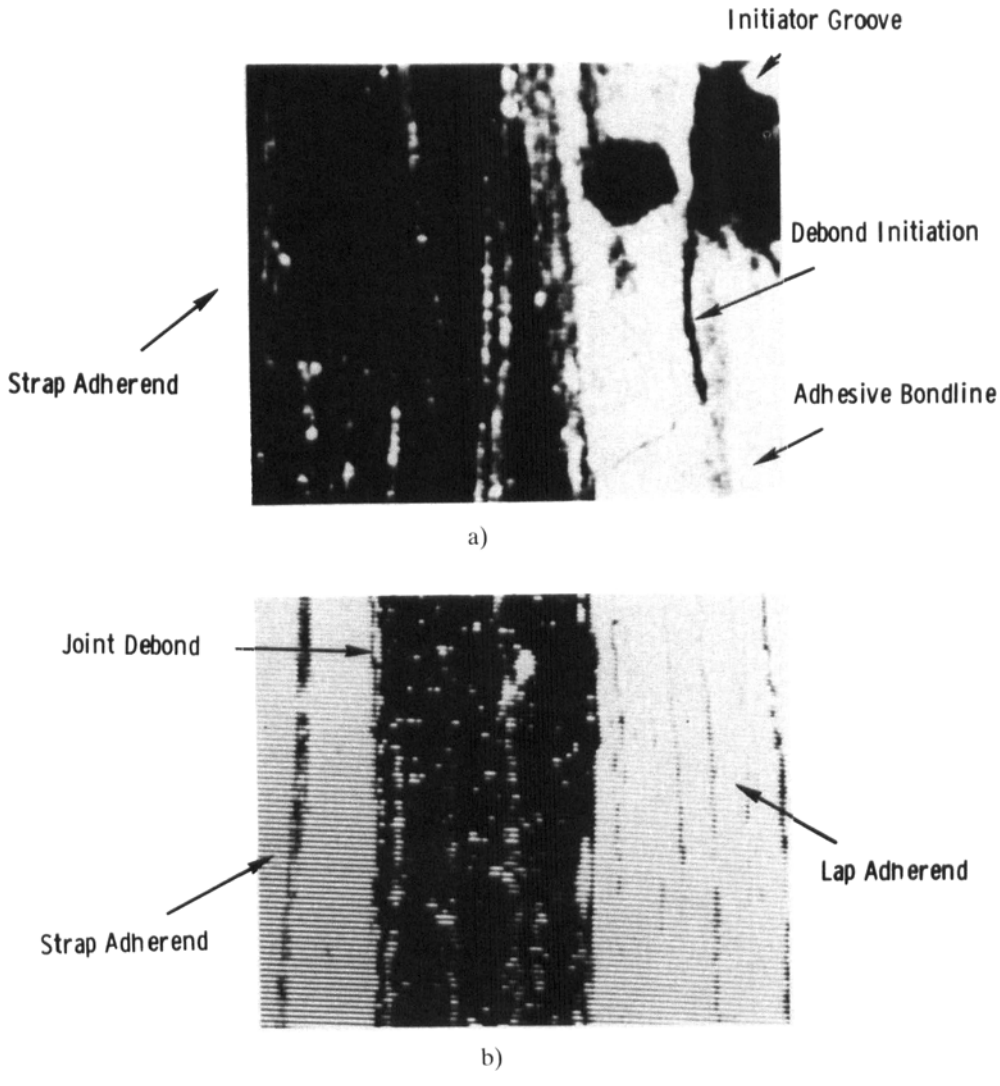

FIGURE 4 Debond Initiation and Growth Characteristics for a Primed Joint (Bondline Thickness = 0.813 mm): a), Debond Initiation at Groove; b), Primer/Adherend Debonding after Initiation.

Finite Element Modeling Procedures

The boundary conditions employed for the present study are illustrated in Fig. 6a. The constraints placed at the fixed and loaded ends of the joint simulate the grip conditions used in the experiments. The SFE method used eight-node isoparametric elements in regions from the debond front and eight, six-node triangular elements of the variable singularity type[6] at the debond front, as illustrated in Fig. 6b. The notch grooved into the specimen for debond initiation gave a debond front that was

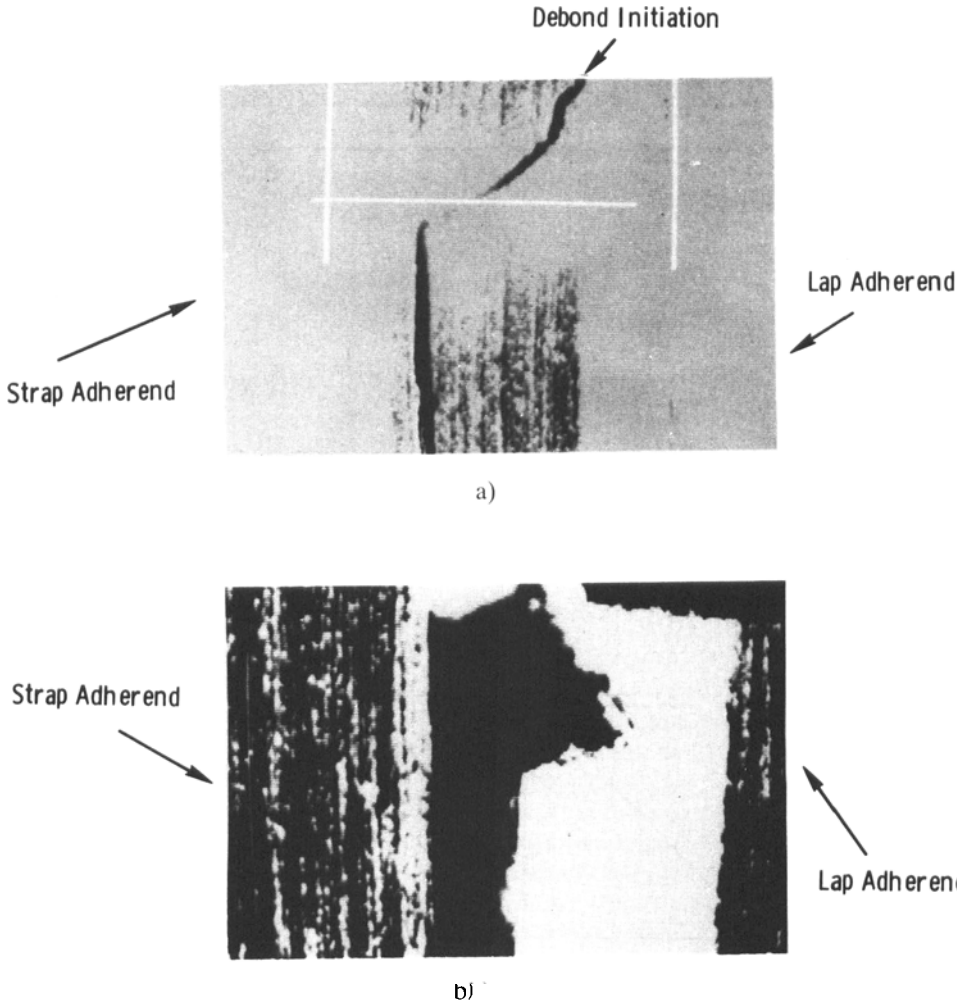

FIGURE 5 Characteristic Debond Initiation and Growth for an Unprimed Joint (Bondline Thickness = 1.27 mm): a), Initiation at Lap Side Interface; b), Debond Opening after 102 mm of Crack Growth.

modeled as sharp crack. The singular element is conformable with adjacent eight-node isoparametric elements. A typical finite element model for the CLS joint using the SFE modeling procedure consisted of 1212 isoparametric elements. Five elements were used with a nonuniform through-the-thickness distribution to model the steel adherend thickness. Four elements were used to model the primer layer. The number of elements used to model the adhesive bondline thickness was seventeen, determined from the mesh sensitivity study described in a following section of the paper.

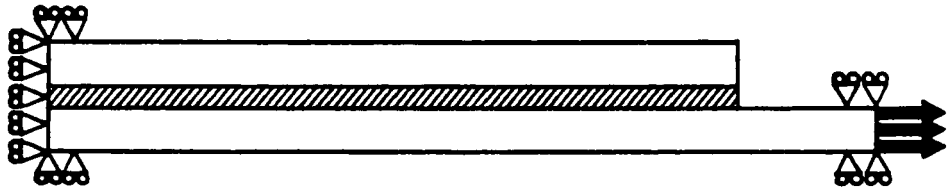

a)

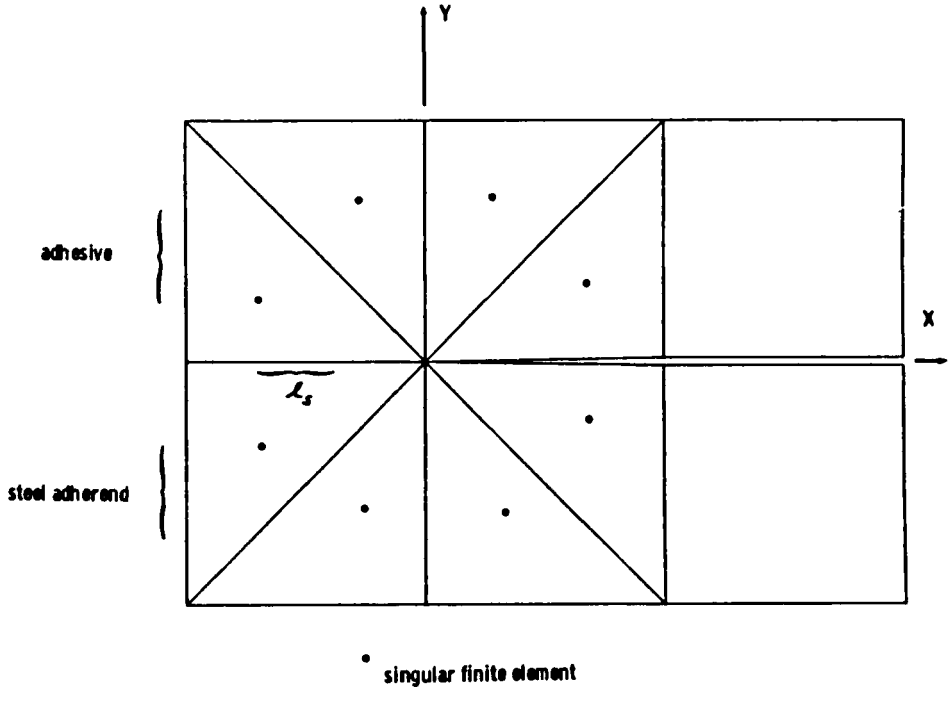

b)

FIGURE 6 Global Boundary Conditions and Local Finite Element Model for CLS Joint: a), Boundary Conditions; b), Local Model for SFE Method.

Mixed-Mode Debond Parameter Formulation

Debond parameters that describe mixed-mode behavior of the CLS joint are the total strain energy release rate, G_t, and its components, G_i and G_{ii}, the opening and shear mode release rates, respectively. The SFE method makes use of displacement fields near the debond tip to determine the mixed-mode parameters. The method is based on a formulation originally derived by Smelser.[7] Crack flank displacements along the upper and lower debond faces are needed to apply the method. Displace-

ments near the debond front are represented in a six-node singular finite element as

$$u = C_u r^{1/2}, v = C_v r^{1/2} \tag{1}$$

where the coefficients C_u and C_v are determined directly from the finite element solution along rays which correspond to the sides of the singular element surrounding the crack tip. The u and v displacements in Eq. (1) correspond to sliding and opening crack flank displacements for the cartesian coordinate system shown in Fig. 6b. The crack opening displacements can then be calculated as

$$\Delta u = (C_u^+ - C_u^-) r^{1/2}, \Delta v = (C_v^+ - C_v^-) r^{1/2} \tag{2}$$

where the plus and minus superscripts signify the upper and lower debond faces, respectively.

The total strain energy release rate as a function of component stress intensity factors, K_i and K_{ii}, was determined by Smelser to be of the form[7]

$$G_t = \frac{1}{16}(\Lambda_1 + \Lambda_2)(K_I^2 + K_{II}^2) \tag{3}$$

where Λ_1 and Λ_2 are defined in the Appendix.

The component values of G_t, G_i and G_{ii}, can be computed as functions of the C_u and C_v coefficients. Previous work directed at applying Smelser's formulation to static CLS joint response[1] derived expressions for G_t, G_i, and G_{ii} which are functions of ΔC_u and ΔC_v, defined in Eq. (2), and K_i and K_{ii}. These expressions, summarized below, are used for computing debond parameters for the CLS joints.

$$G_t = \frac{2\lambda_o^2}{(\Lambda_1 + \Lambda_2)}\{\Delta C_u^2 + \Delta C_v^2\} \tag{4}$$

$$G_i = \frac{1}{16}[\Lambda_1 + \Lambda_2]K_I^2 \tag{5}$$

$$G_{ii} = \frac{1}{16}[\Lambda_1 + \Lambda_2]K_{II}^2 \tag{6}$$

The component stress intensity factors in Eqs. (5)–(6) can be expressed as

$$K_i = \frac{4\sqrt{2}\lambda_o}{\Lambda_1 + \Lambda_2}(\Delta C_u^2 + \Delta C_v^2)^{1/2}\cos\beta \tag{7}$$

$$K_{ii} = \frac{4\sqrt{2}\lambda_o}{\Lambda_1 + \Lambda_2}(\Delta C_u^2 + \Delta C_v^2)^{1/2}\sin\beta \tag{8}$$

The parameters λ_o and β in Eqs. (4)–(8) are defined in the Appendix. The β parameter is dependent on an arbitrary length dimension measured from the debond tip. As discussed in the Appendix, the invariance of the mode mix (K_i/K_{ii}) with respect to this length dimension must be verified when applying the SFE method. The VISTA finite element code[8] was used in this study to apply the SFE

method to analyze the CLS specimens and the above formulation has been incorporated into VISTA.

Mesh Sensitivity Results

Previous studies[1,9] have shown computations for G_i and G_{ii} to be more sensitive to mesh size at the debond tip than are computations for G_t. Therefore, a mesh sensitivity study was conducted for the CLS geometries to determine the influence of the number of through-the-thickness elements on G_t and the mode mix (G_i/G_{ii}). The results are illustrated in Fig. 7. While the results for G_t are relatively insensitive to the number of through-the-thickness elements, the G_i/G_{ii} ratio is strongly dependent on the number of elements. As a result of this study, 17 elements were used to model the bondline thickness of the CLS joint. The number of bondline elements along the specimen length and in the vicinity of the debond tip was increased to preserve the aspect ratio of the singular element. This increase gave an l_s value of 0.00635 mm for the side of the singular element shown in Fig. 6b.

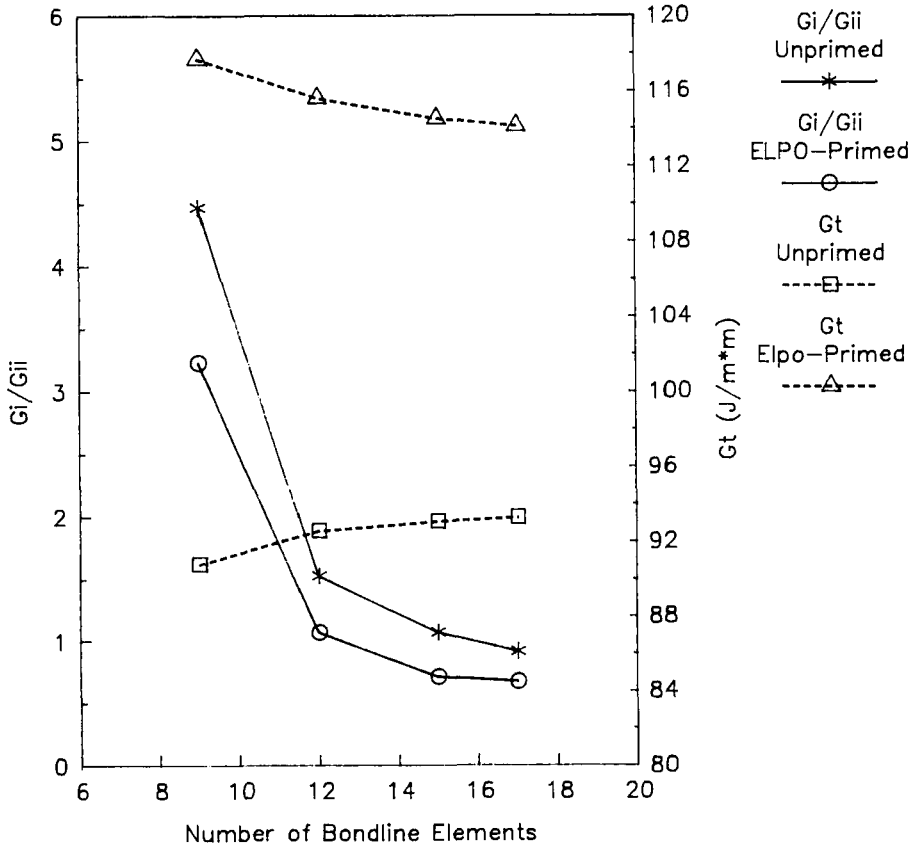

FIGURE 7 Through-The-Thickness Mesh Size Dependence of G_t and G_i/G_{ii} (Bondline Thickness = 0.305 mm, a = 3.2 mm).

RESULTS FOR MIXED-MODE CYCLIC DEBONDING

For the computational studies, minimum and maximum load values corresponding to measured debond growth rates, *da/dN*, were input into the VISTA program to compute ΔG values using the following expressions.

$$\Delta G_t = G_t|_{P=P_{max}} - G_t|_{P=P_{min}} \tag{9}$$

$$\Delta G_i = G_i|_{P=P_{max}} - G_i|_{P=P_{min}} \tag{10}$$

$$\Delta G_{ii} = G_{ii}|_{P=P_{max}} - G_{ii}|_{P=P_{min}} \tag{11}$$

Fig. 8 shows results for ΔG_t, ΔG_i, ΔG_{ii}, and mode mix ($\Delta G_i/\Delta G_{ii}$) as a function of debond length for a CLS specimen with a 0.305 mm bondline thickness, tested at a ΔP load level of 12.77 kN. The curves for the unprimed (Fig. 8a) and primed (Fig. 8b) condition show slight increases in total and component ΔG values over the 102 mm of debond growth for each CLS specimen. The mode-mix ratios are constant over the considered range of debond lengths. As a result of the slight increases in ΔG values over the observed debond growth range, averaged ΔG values were used for cyclic growth comparisons based on computed release rates at debond lengths equal to 25.4, 45.7, 66.0, and 86.4 mm.

A study was completed to determine if one of the components of strain energy release rate dominates the cyclic debonding behavior of the CLS joints. The debond growth rates that were measured in the testing program were above threshold values in that cyclic debonding occurred and below critical values in that rapid debonding of the specimens did not occur. Correlations between debond growth rates and change in strain energy release rate over one load cycle were therefore sought which had the form

$$da/dN = A\Delta G^b \tag{12}$$

where A and b are material properties that characterize the fatigue behavior of the adhesive system for the mode-mix ratio specific to the CLS joint.

Correlations between *da/dN* and ΔG are shown in Figs. 9 and 10 for unprimed and primed CLS specimens, respectively. A least squares regression analysis was used to fit the data to an expression of the form given by Eq. (12). The determination of threshold strain-energy release rate ranges for debond initiation and threshold ranges for catastrophic debond propagation were excluded from this study. The power law form is appropriate for the debond growth rate regime for tests with artificially-induced cracks in the adhesive layer. Other investigators[10,11] have applied this debond growth model with similar experimental sample sizes to characterize CLS joint behavior. The power law equation was fitted to the data for each type of specimen to determine if the form of the relationship was appropriate. The correlation coefficient of the least squares fit, the power law exponent, b, and the power law coefficient, A, are summarized in Tables II–IV for the unprimed and primed specimens with bondline thicknesses equal to 0.305, 0.813, and 1.27 mm, respectively. Equation (12) seems to provide a good fit to the data and, therefore, is an

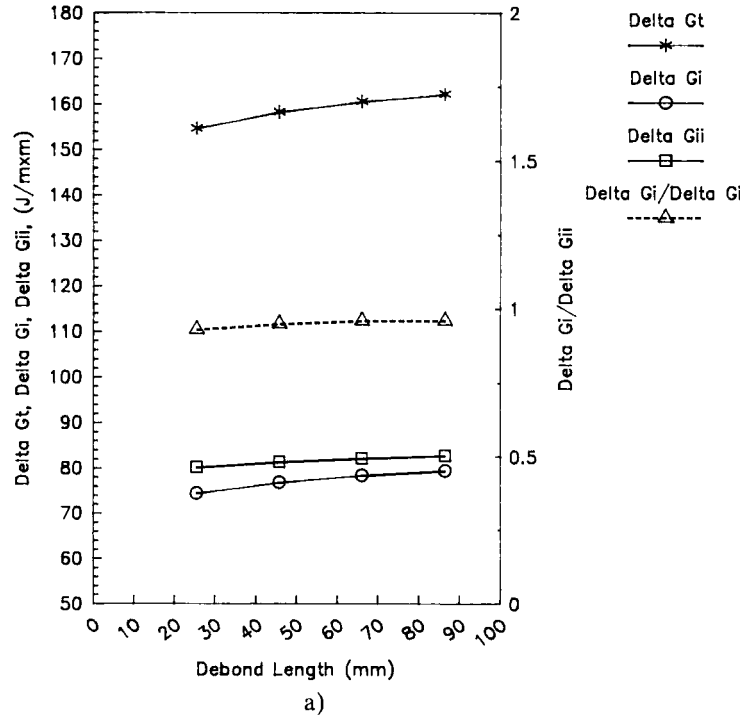

a)

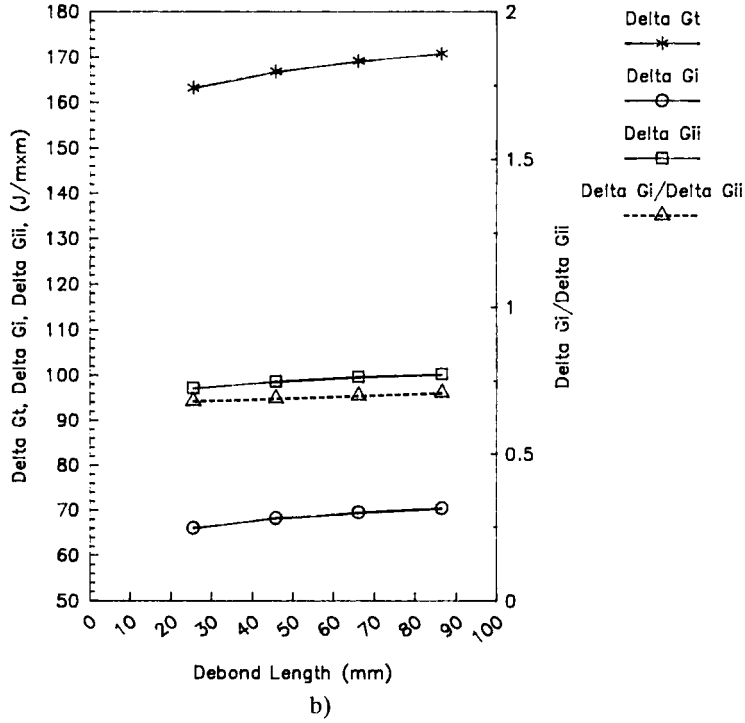

b)

FIGURE 8 Results for Strain Energy Release Rate and Mode Mix *vs.* Debond Length (Bondline Thickness = 0.305 mm, $\Delta P = 12.77$ kN): a) Unprimed; b) Primed.

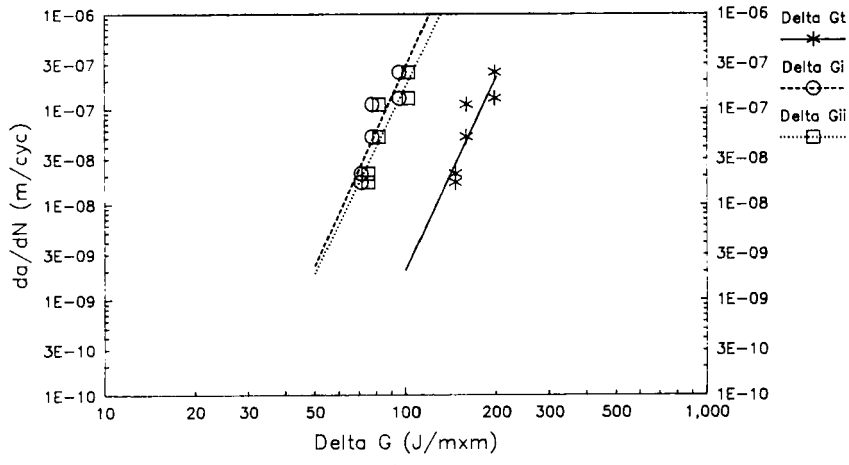

a)

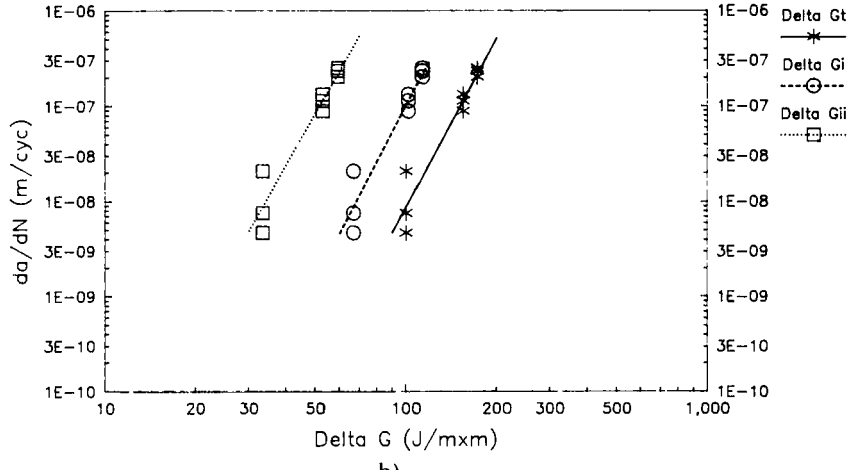

b)

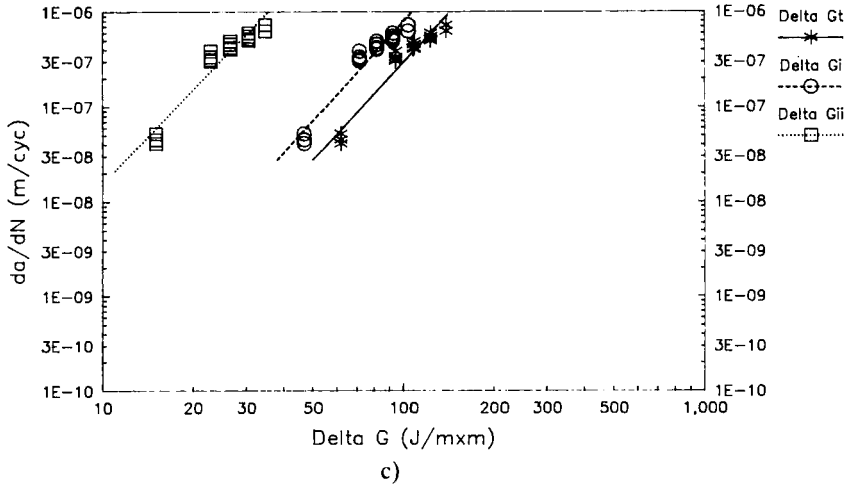

c)

FIGURE 9 *da/dN vs.* ΔG_i, ΔG_{ii}, and ΔG_t for Unprimed Joints: Bondline Thickness = a), 0.305 mm; b), 0.813 mm; c), 1.27 mm.

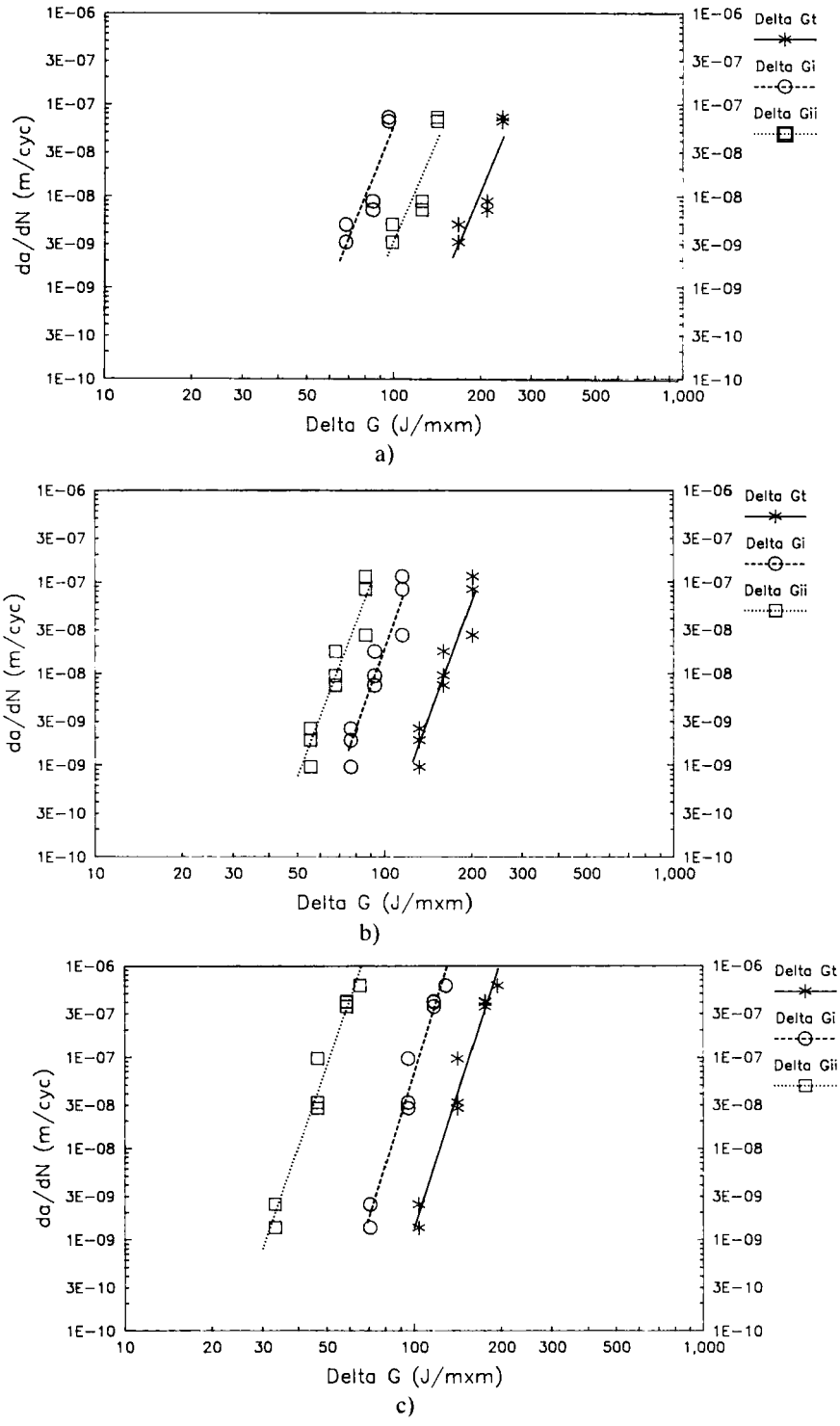

FIGURE 10 *da/dN vs.* ΔG_i, ΔG_{ii}, and ΔG_t for Primed Joints: Bondline Thickness = a), 0.305 mm; b), 0.813 mm; c), 1.27 mm.

TABLE II
Power law fit parameters for CLS specimen with 0.305 mm bondline thickness

	Unprimed joints ΔG_t	ΔG_i	ΔG_{ii}
Exponent b	6.732	6.967	6.526
Coefficient A	7.1×10^{-23}	3.3×10^{-21}	1.5×10^{-20}
Correlation coefficient	0.777	0.783	0.773
	Primed joints ΔG_t	ΔG_i	ΔG_{ii}
Exponent b	7.489	7.906	7.225
Coefficient A	6.7×10^{-26}	9.1×10^{-24}	1.2×10^{-23}
Correlation coefficient	0.793	0.807	0.785

TABLE III
Power law fit parameters for CLS specimen with 0.813 mm bondline thickness

	Unprimed joints ΔG_t	ΔG_i	ΔG_{ii}
Exponent b	5.885	6.060	5.572
Coefficient A	1.5×10^{-20}	7.7×10^{-20}	2.9×10^{-17}
Correlation coefficient	0.931	0.930	0.931
	Primed joints ΔG_t	ΔG_i	ΔG_{ii}
Exponent b	8.608	8.925	8.210
Coefficient A	9.8×10^{-28}	2.7×10^{-26}	8.6×10^{-24}
Correlation coefficient	0.901	0.902	0.900

TABLE IV
Power law fit parameters for CLS specimen with 1.27 mm bondline thickness

	Unprimed joints ΔG_t	ΔG_i	ΔG_{ii}
Exponent b	3.429	3.479	3.287
Coefficient A	4.1×10^{-14}	8.8×10^{-14}	8.0×10^{-12}
Correlation coefficient	0.932	0.936	0.921
	Primed joints ΔG_t	ΔG_i	ΔG_{ii}
Exponent b	9.774	10.161	9.063
Coefficient A	3.9×10^{-29}	3.2×10^{-28}	3.3×10^{-23}
Correlation coefficient	0.967	0.968	0.967

appropriate choice for comparing the debond characteristics of joints with different bondline thicknesses. Furthermore, for the unprimed and primed specimens, the values of the correlation coefficient are about the same for G_i, G_{ii}, and G_t. This indicates that debond growth rate is a function of the combined effects of G_i and G_{ii}. Thus, the total strain energy release rate is an appropriate debond parameter in making debond growth comparisons between CLS joints of different bondline thicknesses and surface treatments.

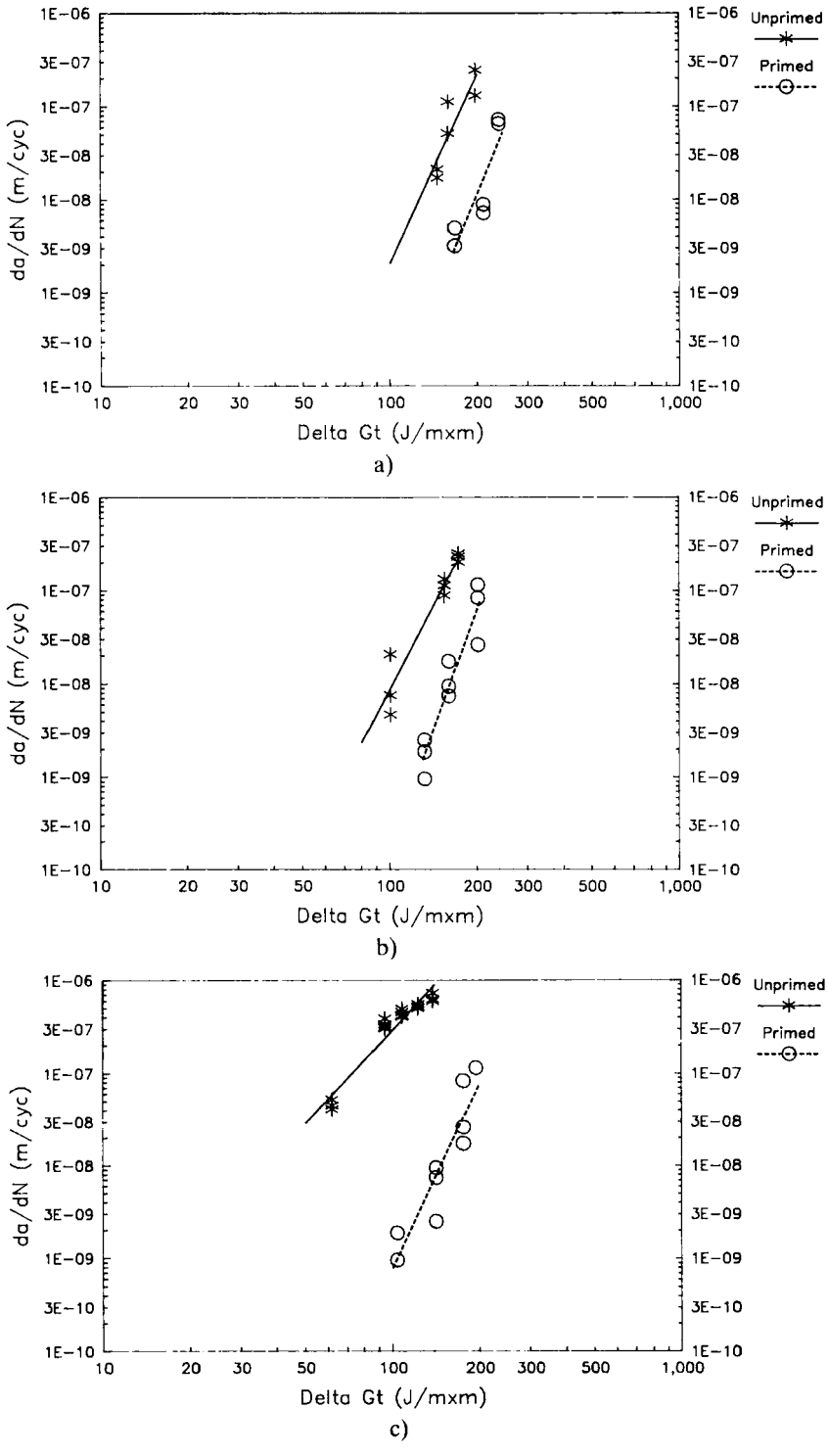

FIGURE 11 Comparison of *da/dN vs.* ΔG_t Results for CLS Joints: Bondline Thickness = a), 0.305 mm; b), 0.813 mm; c), 1.27 mm.

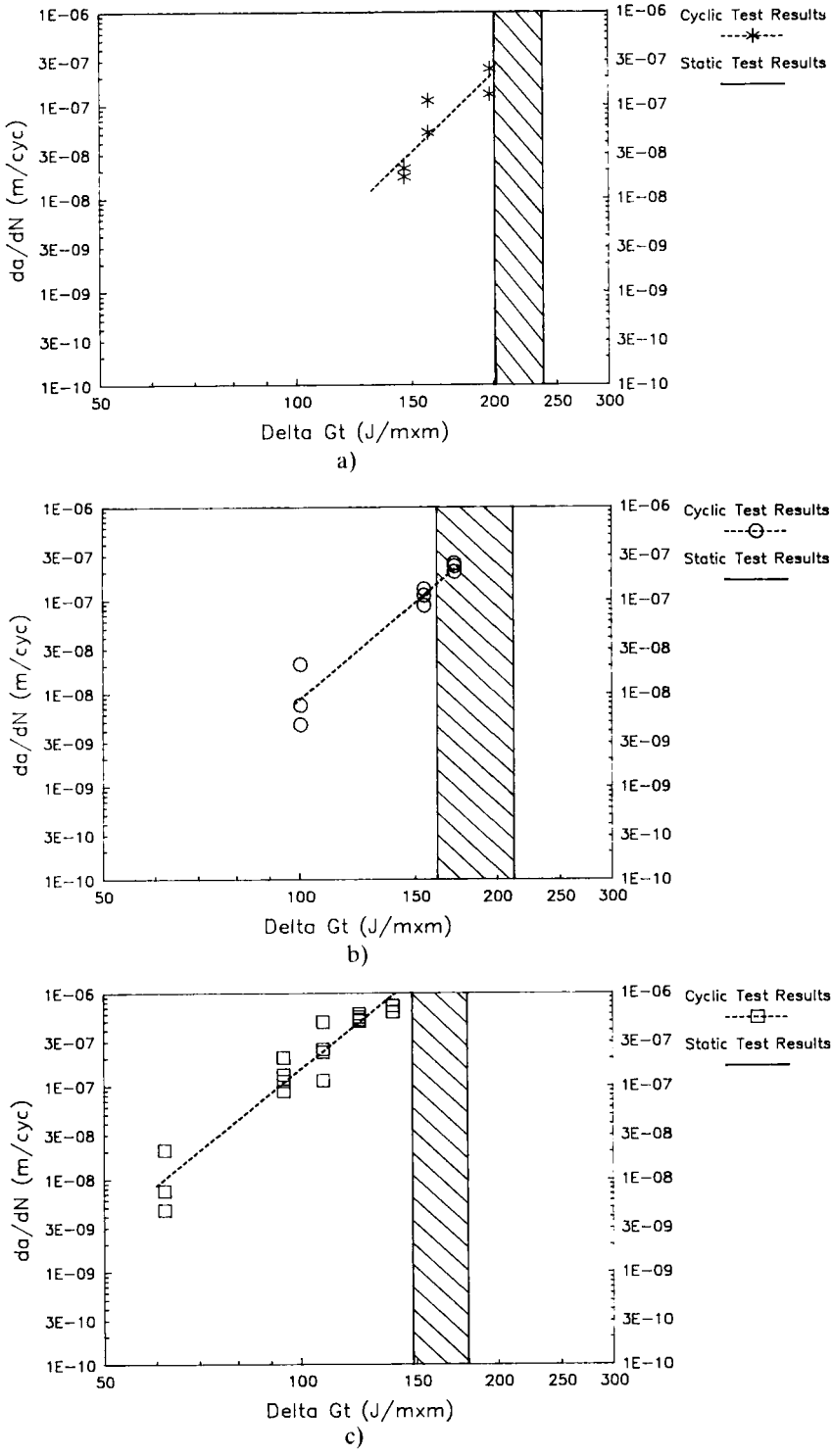

FIGURE 12 Comparison of Static and Cyclic Debond Results for Unprimed CLS Joints: Bondline Thickness = a), 0.305 mm; b), 0.813 mm; c), 1.27 mm.

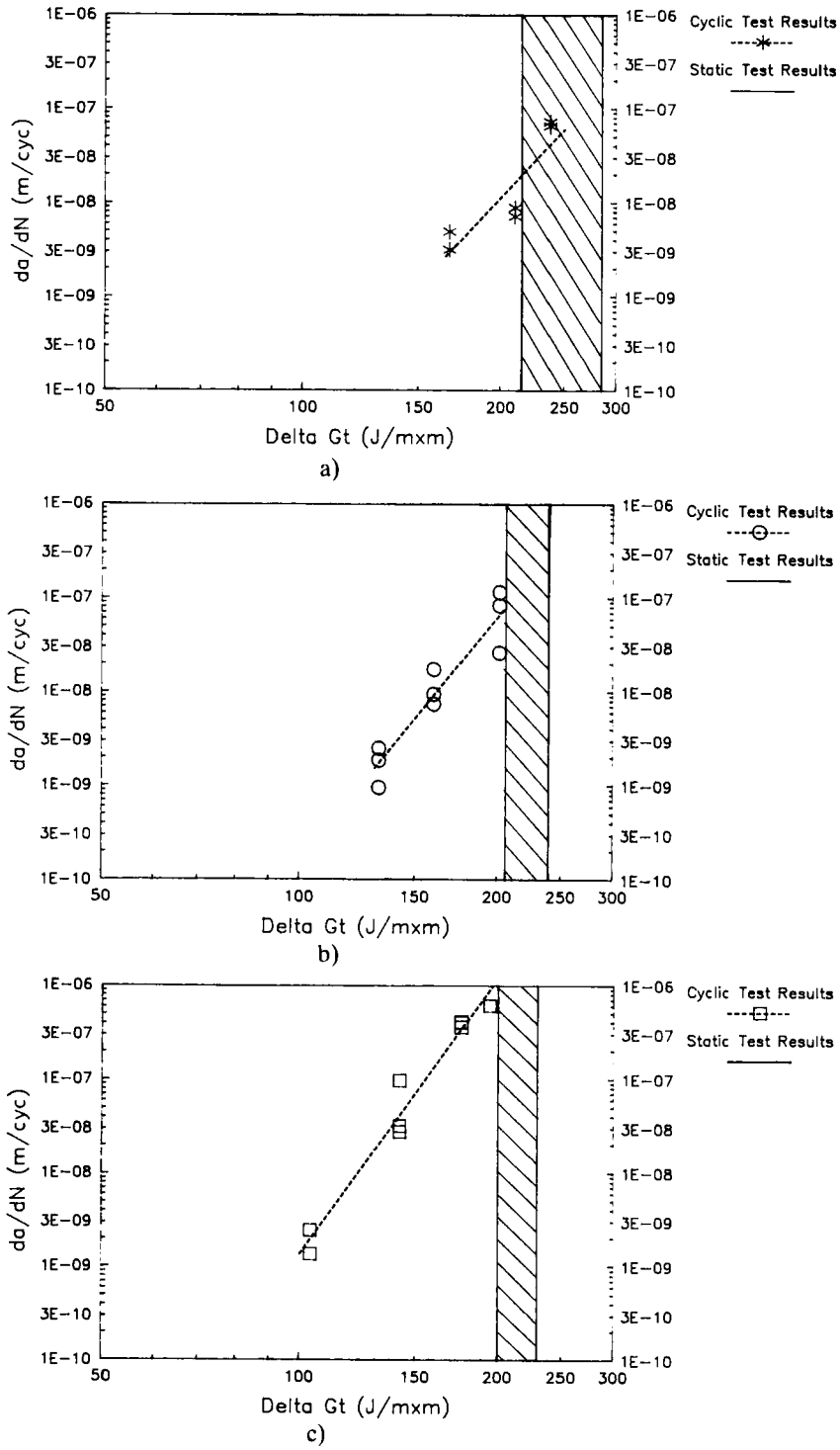

FIGURE 13 Comparison of Static and Cyclic Debond Results for Primed CLS Joints: Bondline Thickness = a), 0.305 mm; b), 0.813 mm; c), 1.27 mm.

The results presented in Tables II-IV show a significant influence of bondline thickness on the magnitude of the power law exponent, b. For the unprimed specimens, the exponent decreased with increasing bondline thickness. The exponent for ΔG_t decreased by 12.6% when the bondline thickness was increased from 0.305 to 0.813 mm. However, a more significant decrease of 41.7% occurred when the bondline was increased from 0.813 to 1.27 mm. For the primed specimens, the exponent increased with increasing bondline thickness. The power law exponent for ΔG_t increased by 14.9% when the bondline thickness was increased from 0.305 to 0.813 mm. An increase of 13.5% occurred when the bondline was increased from 0.813 mm to 1.27 mm.

The values of b determined from this study ranged from 3.4 to 6.7 for the unprimed specimens and from 7.5 to 9.7 for the primed joints. These values are quite high compared with typical values[12] of b for fatigue crack growth in aluminum and steel alloys which range from 1.5 to 3. These steep slopes mean that a small change in applied load would cause a large change in debond growth rate. Thus, debond propagation in CLS adhesive joints is more sensitive to errors in design loads than are typical cracks in metallic structures.

Priming the CLS adherend joint surfaces significantly increased ΔG_t values corresponding to a constant debond growth rate. As illustrated in Fig. 11, for a debond growth rate equal to 3.0×10^{-8}, priming increased the strain energy release rate values by 53%, 44%, and 242% for bondline thicknesses equal to 0.305, 0.813, and 1.27 mm, respectively. Thus, priming was more effective in increasing adhesive joint resistance to cyclic debonding for the thickest bondlines considered in this study.

Finally, comparisons between ΔG_t values for cyclic loads obtained from this study and G_t values for static loads obtained from a previous study[1] are illustrated in Fig. 12 for unprimed CLS joints and in Fig. 13 for primed CLS joints. The range of G_t values corresponding to static loads represents debond growth from 25 mm to 102 mm, the same range of values used for the cyclic debond growth experiments in the present study. Comparing ΔG_t values for a debond rate of 3.0×10^{-8} with average G_t values over the illustrated ranges shows that cyclic loading caused debond growth at significantly lower ΔG_t values than corresponding values for static loads. Specifically, the unprimed CLS joints had reductions in ΔG_t ranging from 32% for the 0.305-mm bondlines to 54% for the 1.27-mm bondlines. The primed joints had smaller reductions, ranging from 9% for the 0.305-mm bondlines to 36% for the 1.27-mm bondlines. Thus, bonded joint designs which rely only on static strength data can be nonconservative for cyclic load conditions.

CONCLUSION

Fracture mechanics analysis concepts have been applied to evaluate debond behavior of CLS specimens bonded with unprimed and primed adherend surfaces. Tension-tension tests were conducted with a stress ratio (P_{min}/P_{max}) of 0.1 and at a frequency of 10 Hz. Debond growth rates, da/dN, were measured using a remote imaging microscope. Corresponding changes in strain energy release rates were

computed based on a singular finite element formulation. The computations allowed for the determination of the peel component, ΔG_i, and the shear component, ΔG_{ii}, of the total release rate, ΔG_t. Three bondline thicknesses (0.3, 0.8 and 1.3 mm) were evaluated.

When calculated total and component values of ΔG were compared with the measured debond growth rates on log-log plots, a power law relationship of the form $da/dN = A\Delta G^b$ was shown to exist. The power law exponent, b, and the power law coefficient, A, represent material characteristics of the bondline adhesive system which are specific to the CLS specimen mode mix. Fitting the power law relationship to the experimental and computational data using least squares regression analysis showed the values for A and b to be similar for ΔG_t, ΔG_i, and ΔG_{ii}. This suggests that the observed growth rates are functions of the combined effect of ΔG_i and ΔG_{ii}. Therefore, ΔG_t is the appropriate fracture parameter for representing cyclic debond growth of the CLS specimens. Furthermore, priming the CLS joints significantly increased ΔG_t values corresponding to a constant debond rate. For a debond growth rate equal to 3.0×10^{-8}, priming increased ΔG_t values by 53%, 44%, and 242% for bondline thicknesses equal to 0.305, 0.813, and 1.27 mm, respectively.

The values of b determined from this study ranged from 3.4 to 6.7 for unprimed joints and from 7.5 to 9.7 for primed joints. These values are quite high compared with typical values of b for cyclic crack growth in aluminum and steel alloys which range from 1.5 to 3.0. When plotted on a log-log scale, least squares plots relating da/dN to ΔG_t have slopes equal to the power law exponent. Steep slopes mean that a small change in applied load would cause a large change in debond growth rate. Thus, debond growth in CLS adhesive joints is more sensitive to errors in design loads than are typical cracks in metallic structures. As a consequence of these steep slopes, it may be difficult to design structural bonded joints for finite life since minor design changes or small analysis errors could cause a much shorter life than a specified design value. A viable alternative would be an infinite life design approach.

Finally, cyclic loading caused debond growth at significantly lower values of ΔG_t than corresponding values for static loads. The unprimed joints had reductions in ΔG_t ranging from 32–54%, while the primed joints had reductions in ΔG_t ranging from 9–36%. Thus, static data alone are insufficient to form a basis for the design of structural adhesively-bonded joints. Instead, ΔG_t values associated with very slow rate cyclic debonding may be more appropriate for joint design and adhesive selection.

Acknowledgments

The author would like to thank Jack Melichar for designing the specimen grips and conducting the cyclic debond tests.

References

1. D. W. Schmueser and N. L. Johnson, *J. Adhesion* **32,** 171 (1990).
2. S. Mall, M. Rezaizadeh, and R. Gurumurthy, *J. Eng. Mat. And Tech.* **109,** 17 (1987).
3. W. S. Johnson and S. Mall, "A Fracture Mechanics Approach for Designing Adhesively Bonded

Joints," in *Delamination and Debonding of Materials,* **ASTM STP 876,** W. S. Johnson, Ed. (American Society for Testing and Materials, Philadelphia, 1985), p. 189.
4. S. Mall, W. S. Johnson, and R. A. Everett, Jr., "Cyclic Debonding of Adhesively Bonded Composites," in *Adhesive Joints,* K. L. Mittal, Ed. (Plenum Press, New York, 1984), p. 639.
5. J. Romanko, K. M. Liechti, and W. G. Knauss, "Integrated Methodology for Adhesive Bonded Joint Life Prediction," AFWAL-TR82-4139, (1982).
6. M. Stern, *J. Numer. Meth. In Eng.* **14,** 409 (1979).
7. R. L. Smelser, *Int. J. Fracture* **15,** 135 (1979).
8. E. B. Becker, R. S. Chambers, L. R. Collins, W. G. Knauss, K. M. Liechti, and J. Romanko, "Viscoelastic Analysis of Adhesively Bonded Joints Including Moisture Diffusion," AFWAL-TR-84-4057, (1984).
9. D. Ginsburg, "Calculation of Fracture Parameters for Interface Cracks with Application to Mixed Mode Crack Initiation," University of Texas EMRL 87/2, (1987).
10. R. A. Everett, Jr. and W. S. Johnson, "Repeatability of Mixed-Mode Adhesive Bonding," in *Delamination and Debonding of Materials,* **ASTM STP 876,** W. S. Johnson, Ed. (American Society for Testing and Materials, Philadelphia, 1985), p. 267.
11. S. Mall and K. T. Yun, *J. Adhesion* **23,** 215 (1987).
12. *Damage Tolerant Design Handbook,* (Battelle Metal and Ceramics Information Center, Columbus, Ohio, 1972).

APPENDIX

A debond extending along the interface between two elastic, isotropic materials can be idealized as an interface crack consisting of an upper debond face ($\alpha = 1$) and a lower debond face ($\alpha = 2$). As shown by Smelser,[7] a complex stress intensity factor, K, for characterizing the stress field near the debond tip is given by

$$K = K_o e^{i\beta} = K_i + iK_{ii} \tag{A1}$$

where K_i and K_{ii} are stress intensity components corresponding to opening and shearing modes, respectively.

These components can be decomposed into

$$K_i = K_o \cos\beta$$

$$K_{ii} = K_o \sin\beta \tag{A2}$$

where

$$K_o = \frac{4\sqrt{2}\lambda_o}{\Lambda_1 + \Lambda_2}(\Delta C_u^2 + \Delta C_v^2)^{1/2} \tag{A3}$$

$$\beta = \epsilon \ln r_o - \delta - \pi/2 - \phi|_{r_o} \tag{A4}$$

$$\tan\phi = \Delta v/\Delta u \tag{A5}$$

and r_o is an arbitrary location at which the components of crack opening displacement, Δv and Δu, are determined.

The constant λ_o is expressed as

$$\lambda_o = \frac{1}{2}(1 + 4\epsilon^2)^{1/2} \tag{A6}$$

where ϵ is the bi-material elastic constant defined by

$$\epsilon = \frac{1}{2\pi} \ln\left[\frac{\mu_1 + \mu_2 \kappa_1}{\mu_2 + \mu_1 \kappa_2}\right] \tag{A7}$$

and

$$\kappa_\alpha = \begin{Bmatrix} 3 - 4\nu_\alpha \text{ Plane Strain} \\ (3 - \nu_\alpha)/(1 + \nu_\alpha) \text{ Plane Stress} \end{Bmatrix}, \alpha = 1,2 \tag{A8}$$

In Eqs. (A7)–(A8), μ_α and ν_α are the shear modulus and Poisson's ratio of material α, respectively.

Furthermore, the material constants Λ_α in Eq. (A3) are defined as

$$\Lambda_\alpha = \begin{Bmatrix} 3 - 4\nu_\alpha)/\mu_\alpha \text{ Plane Strain} \\ 4/\mu_\alpha(1 + \nu_\alpha) \text{ Plane Stress} \end{Bmatrix}, \alpha = 1,2 \tag{A9}$$

while the δ constant in Eq. (A4) is defined as

$$\delta = \tan^{-1}(2\epsilon) \tag{A10}$$

Thus, the individual stress intensity components can be computed using Eqs. (A2)–(A10) once the coefficients ΔC_u and ΔC_v have been determined from the finite element solution.

Using these expressions for K_i and K_{ii}, the total energy release rate can be expressed as

$$G_t = \frac{1}{16}\Lambda_1 + \Lambda_2)(K_i^2 + K_{ii}^2) \tag{A11}$$

Substituting Eqs. (A2)–(A3) into Eq. (A11) gives G_t in terms of the crack flank displacement coefficients

$$G_t = \frac{2\lambda_o^2}{\Lambda_1 + \Lambda_2}(\Delta C_u^2 + \Delta C_v^2)\,. \tag{A12}$$

The determination of K_i and K_{ii} involves an arbitrary length parameter, r_o, which appears in the definition of β in Eq. (A4). Even though r_o and ϵ in Eq. (A4) are very small in magnitude, the $\epsilon \ln r_o$ term is of the same order as $\pi/2$ and ϕ.

Thus, K_i and K_{ii} can vary over selected regions for computing the stress intensity factors. However, the total strain energy release rate is independent of r_o. For the CLS joints considered in this study, a sensitivity study showed that an r_o value equal to 0.025 μm was appropriate for computing the debond parameters.

For the case of cohesive debonding (crack front between similar materials), it can be shown that component values given by Eqs. (A2)–(A3) are independent of r_o. The material constants for cohesive debonding reduce to

$$\epsilon = \delta = 0 \quad , \qquad \lambda_o = 1/2 \tag{A13}$$

Thus,

$$\beta = \left[\frac{\pi}{2} + \tan^{-1}(\Delta C_v/\Delta C_u)\right] \tag{A14}$$

$$\cos\beta = \cos[\tan^{-1}(\Delta C_v/\Delta C_u)]$$

$$= \frac{\Delta C_v}{(\Delta C_v^2 + \Delta C_u^2)^{1/2}} \tag{A15}$$

Similarly,

$$\sin\beta = \frac{\Delta C_u}{(\Delta C_v^2 + \Delta C_u^2)^{1/2}} \tag{A16}$$

Thus, substituting Eqs. (A13)–(A16) into Eq. (A2) gives the following strain energy release rate components for a cohesive bond.

$$G_i = \frac{1}{\Lambda}(\Delta C_v^2) \tag{A17}$$

$$G_{ii} = \frac{1}{\Lambda}(\Delta C_u^2) \tag{A18}$$

Using Eq. (A9) for plane strain and the following relationship between shear modulus and Young's modulus

$$\mu = \frac{E}{2(1+\nu)} \ , \tag{A19}$$

Equations (A17) and (A18) reduce to

$$G_i = \frac{E\Delta C_v^2}{32(1-\nu^2)} \tag{A20}$$

$$G_{ii} = \frac{E\Delta C_u^2}{32(1-\nu^2)} \tag{A21}$$